Simplified modelling and numerical simulations of concrete carbonation in unsaturated conditions

Benoît Bary* — Claude Mügler**

* *CEA/DEN/DANS/DPC/SCCME/Laboratoire d'Etude du Comportement des Bétons et Argiles, Bat. 158, 91191 Gif/Yvette cedex*

benoit.bary@cea.fr
** *CEA Saclay*
Bat. 701 P 2A, 91191 Gif/Yvette cedex
claude.mugler@cea.fr

ABSTRACT. *We present in this paper a simplified modelling of cementitious material carbonation in unsaturated conditions, constituting an enhanced version of the modelling presented in (Bary et al., 2004). The main improvements consist in the introduction of kinetics for the calcite formation evolving as a function of the degradation state and in the adoption of carbonation mechanisms different for portlandite and the other hydrates. Moreover, the three coupled equations governing the system are now solved with a mixed finite element method in the Cast3m code. Numerical simulations are carried out and compared in terms of carbonation depth with accelerated test data obtained in the workgroup Concrete Engineering Barriers headed by ANDRA. The confrontation between experimental and numerical results is globally satisfactory; however the determination of pH profiles with the modelling remains an open problem when dealing with accelerated experimental procedures.*

KEYWORDS: *modelling, concrete carbonation, numerical simulations, unsaturated conditions.*

RÉSUMÉ. *On présente dans cet article un modèle simplifié de carbonatation des matériaux cimentaires en conditions insaturées constituant une version améliorée du modèle décrit dans (Bary et al., 2004). Les principales améliorations consistent en la prise en compte d'une cinétique de formation de la calcite évoluant au cours du processus de dégradation et de mécanismes de carbonatation différents pour la portlandite et les autres hydrates. De plus, les trois équations couplées du système sont maintenant résolues à l'aide d'une formulation d'éléments finis mixtes hybrides dans le code de calcul Cast3m. Des simulations numériques sont effectuées et comparées en terme de profondeur de carbonatation aux données expérimentales obtenues sur essais accélérés dans le cadre du groupe de travail Barrières Ouvragées en Béton II piloté par l'ANDRA. La confrontation des résultats est relativement satisfaisante ; la détermination du profil de pH avec le modèle dans les conditions d'essais accélérés demeure cependant un problème ouvert.*

MOTS-CLÉS : *modélisation, carbonatation des bétons, simulations numériques, conditions insaturées.*

1. Introduction

In the context of nuclear waste management, cementitious materials are currently an attractive option for the construction of engineered barriers and underground structures for interim and long-term disposal. Characterizing the long-term behavior of such materials is then a topic of great concern, which receives much attention by the scientific community. This paper focuses on the carbonation process affecting most of cement-based materials and which can participate to the corrosion of the reinforcing steel, this latter phenomenon being known as a major degradation cause of reinforced concrete structures (Saetta *et al.*, 1995). We present an improved version of the simplified model of carbonation in unsaturated conditions developed in (Bary *et al.*, 2004). This model rests on three coupled nonlinear mass balance equations for the water, the calcium in both liquid and solid phases, and the carbon dioxide in both gaseous and solid phases, respectively. The main improvements concern the introduction of kinetic constants for the calcite formation evolving as a function of the degradation state, and the distinction of the carbonation mechanisms for the portlandite and the other hydrated products. The former aspect results from the decrease of calcite formation rate consecutive to the growing calcite layer which precipitates around the hydrates (especially around the portlandite crystals) and constitutes a diffusive obstacle for carbonate and calcium ions, whereas the latter is due to the reactivity to carbonates which is assumed to be much higher for portlandite. As an important consequence, the carbonation of the main hydrated products is supposed to occur simultaneously but at different rates, contrary to the initial version of (Bary *et al.*, 2004). The three governing equations are solved numerically in 2D in the Cast3m code with a mixed hybrid finite element (MHFE) formulation for the space domain and an implicit scheme in time.

In section 2 of the paper, the governing equations of the system are developed and the main hypotheses of the model are presented. The parameters of this model are identified or fitted to available experimental data, some of them specifically carried out in the framework of the Concrete Engineering Barrier project, as is explained in Section 3. Section 4 presents the simulation results of accelerated carbonation tests performed on cement pastes and concretes with various water to cement (w/c) ratios and initial average saturation degrees. Finally, some concluding remarks are given in section 5.

2. Governing equations

We briefly develop in this section the governing equations of the system, which are widely based on (Bary *et al.*, 2004), with a particular emphasis on the kinetics of calcite formation. As already mentioned, the model is based on the mass balance equations for the water, the carbon dioxide flowing through the gaseous phase and the calcium present in solid phases and pore solution, respectively. Consequently,

the three following variables are assumed to completely define the state of the material regarding the carbonation phenomenon in unsaturated conditions: the saturation degree, the partial pressure of carbon dioxide and the calcium concentration in pore solution (this latter assumed to be directly related to the calcium concentration in the solid phases), which characterize the local water content of the material, the quantity of aggressive substance migrating through the material, and the degradation state of the initial hydrated products, respectively. Both decalcification of the main hydrates and calcite formation resulting from carbonation are introduced in those mass balance equations as source or sink terms. Accordingly, these two mechanisms lead to substantial variations of porosity and consequently of transfer parameters. The main chemical reaction involved in carbonation of cementitious materials is:

$$Ca^{2+} + CO_3^{2-} \leftrightarrow CaCO_3 \qquad [1]$$

where CO_3^{2-} is the predominant carbonate species in pore solution for pH greater than about 10, Ca^{2+} is the calcium ion (which is in equilibrium with the solid phase containing calcium when the reactions are diffusion-controlled) and $CaCO_3$ is calcite.

2.1. *Mass conservation equation for water*

We assume that the water transfer through the connected porosity ϕ of the material results essentially from gradients of capillary pressure arising from the variation of pore water content due for example to drying, as shown by (Mainguy *et al., 2001*) for high performance materials. Consequently, the contribution of the vapour flux is neglected, and the saturation degree S_r completely defines the hydric state of the material. The mass balance equation for the water takes the following form:

$$\frac{\partial \rho_l \phi S_r}{\partial t} = \nabla \cdot [\frac{K(\phi)\rho_l}{\eta} k_{rl}(S_r) \nabla p_l] - M_{H_2O} \frac{\partial \omega_{lS}}{\partial t}, \qquad [2]$$

in which ρ_l is the water mass density, M_{H_2O} is the molar mass of water, p_l and $K(\phi)$ are the pressure of the liquid phase and the intrinsic permeability coefficient, respectively, and $k_{rl}(S_r)$ is the relative permeability for liquid; η denotes the dynamic viscosity of the water, ω_{lS} is the molar concentration (mol/m^3) of water chemically bonded in the solid phase, and $\nabla = (\partial \cdot / \partial x_i) e_i$ where e_i denotes the ith vector of the orthonormal basis. The last term of [2] expresses the water quantity released in the porosity as a consequence of carbonation reactions of the hydrated products (essentially portlandite) of the cement paste. We assume that the pressure of the gaseous phase p_m is negligible with respect to the one of the liquid phase,

such that the capillary pressure $p_c = p_m - p_l \approx -p_l$. The pressure p_l can then be related to S_r with the help of the Kelvin's law:

$$p_c = -p_l = -\rho_l \frac{RT}{M_{H_2O}} \ln\left(h_r(S_r)\right), \quad [3]$$

where $h_r = p_v / p_{vs}$ is the relative humidity, supposed to be related to the saturation degree via the classical isotherm desorption (or adsorption) curves, p_v and p_{vs} are the partial pressure and saturation pressure of the vapour, respectively; R and T are the constant of ideal gas and absolute temperature. The porosity may be written as

$$\phi = \phi_0 + V_d(t) - V_{cal}(t), \quad [4]$$

where $V_d(t)$ and $V_{cal}(t)$ are the current volume fractions of the dissolved hydrated products and the precipitated calcite, respectively. By denoting $\dot{N}_{cal}$ the molar rate of calcite formation per volume of pore solution, $V_{cal}(t)$ may take the form (see (Bary *et al.*, 2004; Bary, 2005) for further details):

$$V_{cal}(t) = V_{CaCO_3} \int_0^t \phi(\tau) S_r(\tau) \dot{N}_{cal}(\tau) d\tau, \quad [5]$$

with V_{CaCO_3} the molar volume of calcite. On the basis of the chemical reaction [1], the rate of calcite formation is classically approached by a first order kinetic law with respect to the calcium and carbonate ions (see e.g. Ishida *et al.*, 2004). As suggested for example in (Atkins, 1998), this law can be simplified by assuming that one of those two ionic species is largely predominant, so that $\dot{N}_{cal}$ may be expressed via the minor specie as:

$$\dot{N}_{cal} = \phi S_r k \; Min\left\{\left\langle C_a - C_a^* \right\rangle, \left\langle C_{\bar{c}} - C_{\bar{c}}^* \right\rangle\right\} = \phi S_r k \min\left(\left\langle C_a - C_a^* \right\rangle, \left\langle p_{\bar{c}} - p_{\bar{c}}^{\,*} \right\rangle k_H\right), \quad [6]$$

where C_a and $C_{\bar{c}}$ are the calcium and carbonate total concentration in pore solution, whereas C_a^* and $C_{\bar{c}}^*$ are the same quantities at chemical equilibrium. $\langle\cdot\rangle$ are the Macaulay brackets, and k is the kinetic coefficient of the reaction; $p_{\bar{c}}$ is the partial pressure of carbon dioxide in the gaseous phase retained as a state variable instead of $C_{\bar{c}}$ in this study (these two quantities are deducible from each other via Henry's law), $p_{\bar{c}}^{\,*}$ is the counterpart of $C_{\bar{c}}^*$ and k_H is the Henry's constant. The values of C_a^* and $C_{\bar{c}}^*$ (or equivalently $p_{\bar{c}}^{\,*}$) are estimated by means of the code CHESS (see e.g. (van der Lee *et al.*, 2003)), which solves in our case the chemical equilibrium equations involved in the carbonation problem. The coefficient k is supposed to evolve as a function of the reaction degree. Indeed, since the formation of calcite occurs preferentially at the surface of the hydrated products, it may form a growing layer acting as a diffusive barrier for the reacting species (namely calcium

and carbonates), in particular around the portlandite crystals. This fact is supported by experimental observations on accelerated tests (see e.g. (Groves *et al.*, 1990)). Moreover, it has been shown that both portlandite and calcium silicate hydrates (C-S-H) phases are submitted to carbonation reaction simultaneously, which is in contradiction with the chemical equilibrium results. As an important consequence, the absence of a clear carbonation front has been noticed. In the following, we adopt the hypothesis that the portlandite and the other hydrates react differently with carbonates. Concerning portlandite, the calcite is supposed to form a growing layer surrounding the diminishing crystals, through which the chemical species involved in the reactions diffuse (see Figure 1). Then, the kinetics of the calcite precipitation from portlandite is controlled by diffusive phenomena, and more precisely by the thickness and the diffusion coefficient D of the calcite layer. Assuming that both initial portlandite crystals and calcite coatings are spherical, the kinetic coefficient k_p for the portlandite takes the following form (Bary, 2005):

$$k_p = \frac{3V_p}{R_{p0}}\left(1-\kappa_p\right)^{2/3}\frac{D}{\left[\lambda + R_{p0}\left(\left(1+\kappa_p\left(V_{CaCO3}/V_{CH}-1\right)\right)^{1/3}-\left(1-\kappa_p\right)^{1/3}\right)\right]} \qquad [7]$$

where $\kappa_p = 1 - V_p/V_{p0}$ with V_p and V_{p0} the current and initial volume fractions of portlandite, respectively; R_{p0} is the initial equivalent radius of portlandite crystals; λ is a parameter interpreted as the initial (virtual) calcite layer depth when $\kappa_p = 0$, that is, when the calcite precipitation initiates (in this situation we then have $k_{p|\kappa_p=0} = 3V_p D/(R_{p0}\lambda)$, which is identified as the kinetic coefficient of calcite formation in solution); V_{CH} is the molar volume of portlandite.

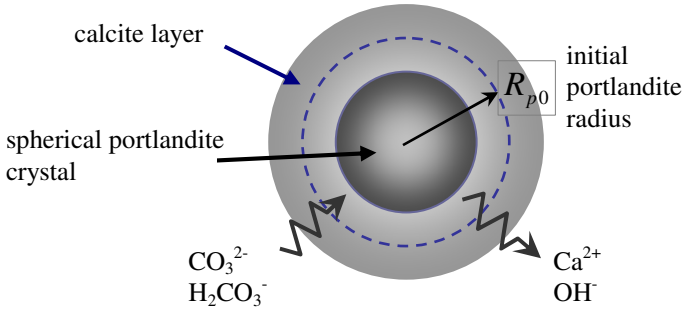

Figure 1. *Schematic illustration of the formation of a calcite layer from an initially spherical portlandite crystal; chemical species diffuse through this layer (after (Thiery, 2005)).*

This approach is similar to the one adopted in (Thiery, 2005); it is also analogous to the modelling of hydration clinker in (Fuji *et al.*, 1974; Bernard *et al.*, 2003). The

other hydrated products (mainly C-S-H and aluminous phases) are supposed to react with the same kinetic coefficient denoted as k_{csh}, such that $k = k_p + k_{csh}$; k_{csh} is assumed to decrease linearly with the current volume fraction of these hydrates for reproducing the effects of the diffusive barrier due to calcite formation. The volume of dissolved hydrates $V_d(t)$ results from two mechanisms: the local precipitation of calcite, and the diffusion of calcium in the pore solution which may dissolve or precipitate solid phases. The former is calculated via the respective kinetic coefficients of the portlandite and the other phases, contrary to the model of (Bary *et al.*, 2004). For example the volume fraction of portlandite transformed locally in calcite $V_{p,\bar{c}}(t)$ is given by

$$V_{p,\bar{c}}(t) = V_{CH} \int_0^t \frac{k_p}{k_p + k_{csh}} \dot{N}_{cal} dt \,, \qquad [8]$$

and the total volume of dissolved portlandite $V_p^d(t) = V_{p,\bar{c}}(t) + V_{p,d}(t)$, with $V_{p,d}(t)$ obtained by the same simplified chemical approach detailed in (Bary *et al.*, 2004). After some manipulations and with the notation $f'(x) = df(x)/dx$, the mass conservation equation [2] can be rearranged as

$$\begin{aligned} &\rho_l \phi \frac{\partial S_r}{\partial t} + \rho_l S_r \frac{\partial V_d}{\partial t} + M_{H_2O} \frac{\partial \omega_{lS}}{\partial t} - \rho_l \phi (S_r)^2 V_{CaCO3} \dot{N}_{cal} \\ &+ \nabla \cdot \left[\frac{K(\phi)\rho_l}{\eta} k_{rl}(S_r) p_c'(h_r) h_r'(S_r) \nabla (S_r) \right] = 0 \end{aligned} \qquad [9]$$

2.2. *Mass conservation equation for carbon dioxide*

The general equation for the mass conservation of carbon dioxide in the gaseous phase takes the form (Bary *et al.*, 2004; Bary, 2005):

$$\frac{\partial \phi (1 - S_r) \rho_{\bar{c}}}{\partial t} = \nabla \cdot \left[f(\phi, S_r) D_{\bar{c}} \frac{M_{\bar{c}}}{RT} \nabla p_{\bar{c}} \right] - M_{\bar{c}} \phi S_r \dot{N}_{cal} \,, \qquad [10]$$

where $\rho_{\bar{c}}$ is the mass density of CO_2 in the gaseous phase, $f(\phi, S_r)$ and $D_{\bar{c}}$ are the reduction factor and diffusion coefficient of CO_2, respectively, such that $f(\phi, S_r) D_{\bar{c}}$ can be viewed as the effective diffusion coefficient of the carbon dioxide through the porous material; $M_{\bar{c}}$ is the molar mass of CO_2. The last term of [10] is the source term describing the dissolution of CO_2 into the liquid phase and its consecutive precipitation into calcite. The equation [10] is established under the hypotheses that the average pressure of the gaseous phase remains quasi constant during the transformations, and that this gaseous phase is composed of carbon dioxide and air, which form an ideal mixture of two ideal gases. Further, the transfer of CO_2 is

supposed to result only from diffusion phenomenon, and is then expressed by the Fick's law; both Knudsen effect and molecular diffusion of carbonates in pore solution are neglected. Making use of the law of ideal gas for CO_2 as $\rho_{\bar{c}} = M_{\bar{c}} p_{\bar{c}} / (RT)$, the mass balance equation for the carbon dioxide [10] can be rewritten as:

$$\begin{aligned} &(1-S_r)\, p_{\bar{c}} \frac{\partial V_d}{\partial t} + \phi(1-S_r)\frac{\partial p_{\bar{c}}}{\partial t} - \phi p_{\bar{c}} \frac{\partial S_r}{\partial t} \\ &+ \phi S_r \dot{N}_{cal}\left(RT - (1-S_r)\, p_{\bar{c}} V_{CaCO3}\right) - \nabla \cdot \left(f(\phi, S_r) D_{\bar{c}} \nabla p_{\bar{c}}\right) = 0 \end{aligned} \quad [11]$$

2.3. *Mass conservation equation for calcium*

The mass conservation equation for the calcium ions in pore solution is expressed in the following form (Bary *et al.*, 2004; Bary, 2005):

$$\frac{\partial \phi S_r C_a}{\partial t} = \nabla \cdot \left[D_a(S_r, \phi) \nabla C_a\right] - \frac{\partial C_{aS}}{\partial t} - \phi S_r \dot{N}_{cal} \quad [12]$$

The term in the bracket describes the flux of molecular diffusion of calcium in pore solution C_a, and is expressed by the classical Fick's law, with $D_a(S_r, \phi)$ the effective diffusion coefficient. The convective part of the flux characterizing the calcium transport due to the movement of water is neglected. C_{aS} is the concentration of calcium in the solid phases initially present in the material, such that $-\partial C_{aS} / \partial t$ corresponds to the molar rate of calcium released by the hydrated products when decalcifying. This quantity is supposed to be directly related to the calcium concentration in pore solution C_a, hence we have $C_{aS}(C_a)$ (see (Bary, 2005) for further details). Finally, the term $-\phi S_r \dot{N}_{cal}$ designates the molar rate of calcium which precipitates in calcite. Using the above notations and definitions, the mass balance equation for the calcium can be recast as:

$$\begin{aligned} &S_r C_a \frac{\partial V_d}{\partial t} + \frac{\partial C_{aS}}{\partial t} + \phi S_r \frac{\partial C_a}{\partial t} + \phi C_a \frac{\partial S_r}{\partial t} \\ &+ \phi S_r \dot{N}_{cal}\left[1 - S_r C_a V_{C_a CO_3}\right] - \nabla \cdot \left(D_a(S_r, \phi) \nabla (C_a)\right) = 0 \end{aligned} \quad [13]$$

3. Identification of the parameters

We present in the sequel the identification and calibration of the model parameters performed on available experimental results, some of them obtained in the framework of the workgroup Concrete Engineered Barrier by different research institutes (the corresponding procedures and complete data are presented in more

details in other contributions of this special issue), on cement pastes and concrete fabricated with CEM I cement. It should be noticed that the same study carried out on specimens made up with CEM V cement, including simulations results of accelerated carbonation tests, is available in (Bary, 2005).

3.1. *Composition of the materials*

As already mentioned, we propose to apply the carbonation modelling developed in section 2 to the case of cement paste and concrete specimens made up with CEM I cement. Three w/c ratios are considered for the cement pastes: 0.30, 0.42 and 0.55, whereas only one is retained for concrete: 0.42. Concrete is simply obtained by mixing sand and aggregates with prescribed proportions to the w/c = 0.42 cement paste formulation (see table 2). The theoretical compositions of all cement pastes (including the one of concrete) are determined under the assumption that the hydrated products are portlandite (CH), C-S-H, monosulfo-aluminate (AFm) and Hydrogarnet (Hyd). Starting from the known chemical composition of the cement, these hydrated phases are calculated with the following formulae (Bary, 2005):

$$\begin{cases} \mathrm{AFm} = \mathrm{S} \\ \mathrm{Hyd} = -1 \times \mathrm{S} + 0.5 \times (\mathrm{Al} - 0.1 \times \mathrm{Si}) \\ \mathrm{CH} = \mathrm{Ca} - 1.65 \times \mathrm{Si} - 4 \times \mathrm{S} - 3 \times \mathrm{Hyd} \\ \mathrm{C\text{-}S\text{-}H} = \mathrm{Si} \end{cases} \quad [14]$$

where S, Si, Al, Ca are the classical notations for the basic chemical species. The basic assumptions underlying this system are that S and Si are totally included in AFm and C-S-H, respectively. CH and Hyd are then determined from Ca and Al quantities. It is moreover supposed that a fraction of Al (or equivalently of Fe, these two species behaving quite similarly regarding the hydration process) corresponding to 10% of C-S-H is incorporated into the C-S-H. The results of the above equations are given in table 1 for the three cement pastes.

w/c	**0.30**	**0.42**	**0.55**
AFm (mol/l)	0.566	0.475	0.404
Hyd (mol/l)	0.241	0.202	0.172
CH (mol/l)	6.860	5.758	4.904
C-S-H (mol/l)	5.328	4.472	3.809
Theoretical total porosity	0.111	0.254	0.364
Mercury accessible porosity	0.11	0.15	0.21

Table 1. *Idealized composition of CEM I cement pastes.*

	Concrete w/c = 0.42
Cement (kg/m^3)	400
Water (kg/m^3)	168
Sand 0/5 (kg/m^3)	858
Aggregates 5/12.5 (kg/m^3)	945
Mass density (kg/m^3)	2371
Volume fraction of paste	0.299
Theoretical total porosity	0.0772
Mercury accessible porosity	0.07

Table 2. *Composition of the concrete with w/c = 0.42.*

For the concrete, the hydrated products of table 1 corresponding to w/c = 0.42 have to be corrected by the volume fraction of the cement paste; its mix proportions are indicated in table 2. It is worth noticing that this concrete has a compression characteristic strength at 28 days (measured on 16×32 cm^2 cylinders) of 72 MPa. For information, the porosity accessible to mercury is given for all materials (Aït-Mokhtar *et al.*, 2006). Since these experimental data appear quite low for w/c = 0.42 and 0.55, and provided that the porosities obtained by water saturation are not known, the theoretical values of porosity will be systematically used for the numerical simulations.

3.2. *Permeability*

The intrinsic permeability K and relative permeability k_{rl} for liquid entering into [9] are chosen as (van Genuchten, 1980):

$$K(\phi) = K_0 \left(\frac{\phi}{\phi_0} \right)^3 \left(\frac{1-\phi_0}{1-\phi} \right)^2 \text{ and } k_{rl}(S_r) = \sqrt{S_r} \left(1 - \left(1 - S_r^{1/m} \right)^m \right)^2, \quad [15]$$

where K_0 is the intrinsic permeability corresponding to the porosity ϕ_0, and m is a constant chosen to be equal to 0.5 for all materials, due to the lack of experimental identification. K_0 is calibrated numerically on experiments carried out for determining the desorption isotherm curves of the materials. The procedure for these tests consists in subjecting the specimens to a (small) change of relative humidity and to measure the evolution of their total mass variations as a function of time (see for more details (Aït-Mokhtar *et al.*, 2006)). In Figure 2 are presented both experimental and numerical results of such tests for the different materials. The values for K_0 used for the simulations are 7.5×10^{-25}, 1.3×10^{-23} and 7.5×10^{-23} m^2 for the cement pastes with w/c = 0.30, 0.42 and 0.55, respectively, and 2.5×10^{-24} m^2 for the concrete. It is worth noting that those values are 2 or 3 orders lower than

the typical values generally reported for similar materials. These differences may be explained by the function retained for k_{rl}, which may not be appropriate and may lead to a significant overestimation of the effective permeability for h_r lower than 0.9. Consequently, in this case the values of K_0 used in the simulations have to be decreased with respect to real ones in order to balance k_{rl} and to more correctly match the experiments, thus leading to the low values identified above. This point would naturally deserve further investigations. Another aspect which may explicate, at least partly, the discrepancies between classical and numerical intrinsic permeability values concerns the quite short durations of drying experiments shown on Figure 2, in particular for the w/c = 0.42 cement paste test. Indeed, when the drying process is insufficiently long, the hydric equilibrium may not be totally reached in the specimen, leading to spurious permeability coefficient (and isotherm desorption) identification. Except for the w/c = 0.55 case, the relatively high slopes of the Figure 2 curves for the highest value of normalized mass decrease indicate that this equilibrium is probably not correctly achieved. Nevertheless, the values identified for K_0 are coherent with the function k_{rl} adopted and lead to satisfactory results in the relative humidity range encountered in practice, as attested by the good agreement between experimental data and numerical simulations of Figure 2.

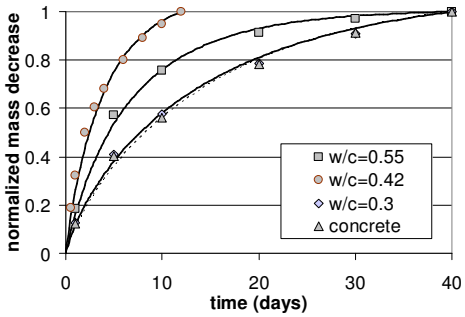

Figure 2. *Evolution of the normalized mass decrease during a drying stage from 90 to 75% h_r (cement pastes with w/c = 0.55 and 0.3 and concrete) and from 75 to 65 % (cement paste with w/c = 0.42): the symbols represent experimental results (Aït-Mokhtar et al., 2006) and the lines numerical ones.*

3.3. *Desorption isotherm curves*

We propose to use the following formulae for expressing the desorption isotherm curves of the materials:

$$h_r = c_2 S_r^{c_1} + c_3 S_r - c_4 S_r^{2} + (1 - c_2 - c_3 + c_4) S_r^{3} \qquad [16]$$

in which c_i are real constants. The fit of these coefficients is performed on experimental data gathered in (Aït-Mokhtar *et al.*, 2006). We present in Figure 3 these results and the corresponding numerical curves for the four considered materials. It is worth mentioning that the experimental data of Figure 3, although well-ordered for the cement pastes, are not in very good accordance with the ones commonly reported in the literature for similar materials (see e.g. Baroghel-Bouny, 1994).

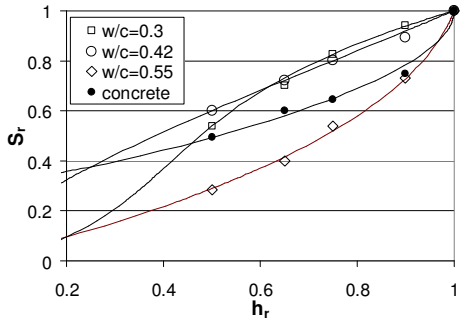

Figure 3. *Numerical desorption isotherm curves (solid lines) and experimental results from (Aït-Mokhtar et al., 2006) (symbols) for the four materials.*

As outlined in the preceding section and as may be supposed from Figure 2, the drying durations during desorption stages were likely insufficient to reach a precise hydric equilibrium, thus leading to a possible alteration of the results. However, although questionable, use will be made of these experimental data in the sequel, in order to ensure a certain homogeneity in all the material data involved in the model. Moreover, since the tests have been carried out for h_r greater than 0.5, the curves are extrapolated for lower h_r values in order to be able to simulate the preconditioning procedure performed on the specimens prior to the accelerated carbonation experiments (again, this extrapolation process may be criticized due to the experimental uncertainties). This procedure permits to impose a prescribed average saturation degree in the whole specimens (see next section and (Aït-Mokhtar *et al.*, 2006)).

3.4. *Initial hydric state of the materials*

As previously mentioned, the specimens are submitted, before the accelerated tests, to a preconditioning procedure aiming at obtaining a given average saturation degree in the material, in order to study the impact of the hydric state on carbonation mechanisms. Three values of saturation degree are retained: 0.65, 0.80 and 0.95. The

process adopted for this preconditioning consists firstly in drying the specimens in a ventilated oven, up to obtain the prescribed average saturation degrees (control is performed on mass). This drying process is accelerated by imposing a temperature of 40° C for the cement pastes and 60° C for concrete. Then, the samples are sealed and subjected to a homogenization phase during 14 days at the same temperature of 40 and 60° C (see (Aït-Mokhtar *et al.*, 2006) for further details). Since it is of great importance to estimate as precisely as possible the initial saturation degree profiles in the specimens at the beginning of the carbonation tests, the complete drying procedure is simulated numerically for all materials with the help of equation [9]. Accordingly, the values of ρ_l, p_{vs} and η for the temperatures $T = 40$ and $T = 60$ ° C are required. We propose to adopt the following expressions due to (Pezzani, 1988) for ρ_l and p_{vs}, and to (Ranznjevic, 1970) for η:

$$\rho_l(T) = 314.4 + 685.6\left[1 - \left(\frac{T - 273.15}{374.14}\right)^{1/0.55}\right]^{0.55} \quad [\text{kg.m}^{-3}],$$

$$p_{vs}(T) = p_{atm} \exp\left[4871.3\frac{T - 100}{373.15(T + 273.15)}\right] \quad [\text{Pa}], \qquad [17]$$

$$\eta(T) = 2.414\times10^{-5} \exp\left(\frac{570.58058}{T + 133.15}\right) \quad [10^{-6}\ \text{kg.m}^{-1}.\text{s}^{-1}].$$

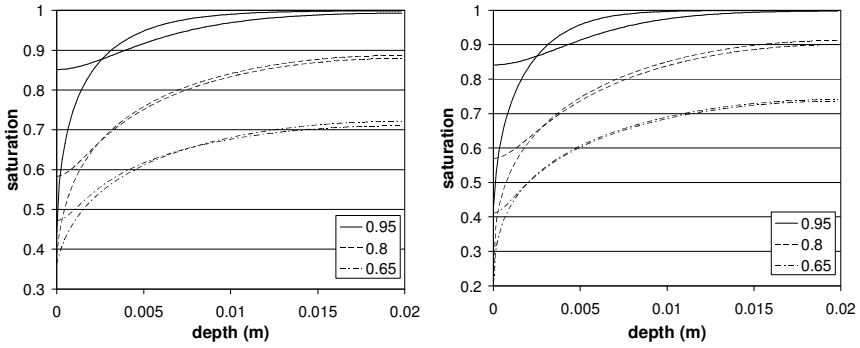

Figure 4. *Numerical saturation degree profiles at the end of both drying and homogenization stages for the prescribed average S_r = 0.65, 0.80 and 0.95, and for the cement pastes with w/c = 0.42 (left) and 0.55 (right).*

To illustrate the obtained numerical results, Figure 4 presents the simulated saturation degree profiles for cement pastes with w/c = 0.42 and 0.55, at the end of

both drying and homogenization stages. The transfer mechanisms are one-dimensional due to the sample preparation; the simulations are carried out on half of the specimen (4 cm length), with a symmetry condition for flux at $x = 0.02$. It can be observed that at the end of the homogenization phase (i.e. at the beginning of the carbonation tests), the computed profiles cannot be considered as homogeneous, in particular for lower initial average saturation degree. It is thus important to correctly estimate them.

3.5. *Diffusion coefficient of CO_2*

We propose to calibrate the diffusion coefficient of CO_2 on experimental data of H_2 diffusion obtained by (Sercombe *et al.*, 2006) on two CEM I cement pastes with w/c = 0.35 and 0.45 (the cement is different from the one used in our study). The CO_2 diffusion coefficients are deduced from the H_2 ones by correcting them with the factor $(M_{H2}/M_{CO2})^{0,5} \approx 0.213$, with M_i the molar mass of gas i (Papadakis *et al.*, 1991). The experimental results of D_{H2} as a function of h_r shown in Figure 5 exhibit two important variations, one around $h_r = 0.8$ and the other one around $h_r = 0.95$. These latter can be explained by the progressive saturation of the capillary porosity for h_r greater than 0.75-0.8, this pore domain being dominant for the diffusion phenomenon in gaseous phase. When the material is close to the total saturation, the value of the diffusion coefficient approaches the one of species in the pore solution. We propose to adapt the expression of (Millington, 1959) giving the evolution of the reduction factor entering into [10] as $f(\phi, S_r) = \phi^{4/3}(1-S_r)^{10/3}$, by replacing S_r by h_r. Two distinct functions are used for more correctly matching the experimental data, one for $h_r \leq 0.82$ and the other for $h_r > 0.82$. The corresponding numerical results for D_{H2} are shown in Figure 5.

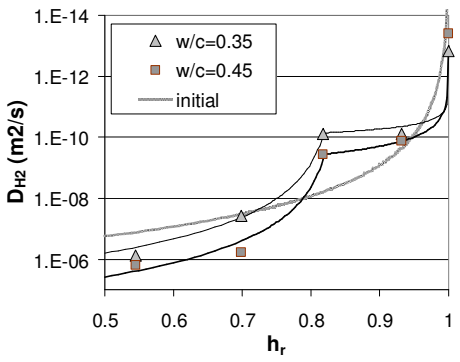

Figure 5. *Numerical evolutions of the diffusion coefficient of H_2 versus relative humidity (solid lines) and experimental results from (Sercombe et al., 2006) (symbols) for two cement pastes.*

The curve referenced 'initial' corresponds to the direct application of Millington's formula (as in (Bary *et al.*, 2004)), which leads to important differences with the experiments. For the materials considered in this study, we suppose that the cement pastes with w/c = 0.30 and 0.42 have diffusion parameters similar to the ones tested in (Sercombe *et al.*, 2006). For the paste with w/c = 0.55, the diffusivity is obtained from the two other cases by assuming that the diffusion coefficient for the w/c = 0.42 paste is the mean value. The diffusion parameter for the concrete is deduced from the paste with w/c = 0.42 by multiplying it by the volume fraction of the paste.

4. Numerical simulations

4.1 *Presentation of the simulations*

The carbonation modelling is applied to the simulation of accelerated carbonation tests for the three cement pastes (w/c = 0.30, 0.42 and 0.55) having initial average saturation degrees of 0.65, 0.80 and 0.95, and for the concrete with w/c = 0.42 and an initial average saturation of 0.80. The various initial hydric states on the pastes will permit to investigate the impact of different saturation levels on the global carbonation kinetics, keeping in mind that the saturation profiles are not homogeneous within the samples due to the conditioning procedure, as revealed in section 3.4. The saturation profiles determined in Figure 4 will serve as initial hydric conditions for simulating the accelerated carbonation tests. The experimental results are generally presented in terms of carbonation depth as a function of time, as measured by phenolphthalein test. This test indicates the regions where the pH is lower or greater than about 9. However, as observed by (Parrott *et al.*, 1989; Lo *et al.*, 2002) among others, the limit between these two zones does not correspond to the calcite precipitation depth (this latter is generally larger). Accordingly, some CH residuals are commonly detected in the carbonated zones where pH is lower than 9. The reasons may reside in the following aspects: firstly, the chemical reactions may not occur instantaneously due to the significant decrease of the kinetic constant of calcite formation in relation to the important carbonate flux, as explained by (Thiery, 2005) on the basis of (Groves *et al.*, 1990) observations. Secondly, from CHESS calculations at chemical equilibrium, the pH of a system containing a large amount of alkaline species (like the materials considered here) becomes lower than 9 only when the initial solid phases are totally carbonated. Further calculations with convenient kinetic coefficients for all reactions show different results when the carbonate concentration in pore solution becomes larger than the values imposed at equilibrium. In the sequel, it will then be supposed that the kinetics aspects mainly control the pH of the solution (in the case of accelerated tests): when the carbonates migrating through the material are in excess in relation to the rate able to precipitate with calcium into calcite, this latter being specified by the local kinetic constants, thus the pH drops. Since our simplified model does not permit to precisely describe

the pH, and due to our hypothesis that the reactivity of portlandite is higher than the one of the other hydrates, we assume that the pH limit value of 9 is strongly related to k_p values (see next section).

The three coupled nonlinear governing equations are solved in the Cast3m code in 2D by using a MHFE formulation for the space domain and an implicit scheme in time (Dabbene, 1998; Mügler, 2004). Contrary to the classical FE method, the MHFE scheme is locally conservative, which guarantees a good precision when solving mass conservation-like equations with dissolution/precipitation terms, even in the case of strong spatial variations of physical properties (for example diffusion coefficient).

4.2 *Numerical results*

We present in this section the numerical results concerning the simulations of accelerated carbonation tests performed on the materials described in section 3. Briefly speaking, these tests consist in subjecting the specimens to an external environment at atmospheric pressure and composed of 50% CO_2 and 50% air, at $T = 20$ °C and $h_r = 0.65$. The case of the cement paste with w/c = 0.42 will be more particularly detailed in terms of calcite, portlandite, porosity and saturation degree profiles at different times. The carbonation depths as a function of time will be reported for all materials and compared with experiments. X-ray diffraction (XRD) mineralogical profiles of calcite and portlandite for the cement paste with w/c = 0.42 will also be confronted to their computed counterparts. The parameters entering into the expression [7] of the kinetic coefficient k_p are adjusted to the following values: $D = 5\times10^{-13}$ m^2/s, $\lambda = 5\times10^{-7}$ m and $R_{p0} = 20\times10^{-6}$ m (for simplicity it is supposed that R_{p0} does not change between the different cement pastes, although some experimental results show larger average radius for materials with higher w/c ratios, see e.g. (Chaussadent *et al.*, 2001)); k_{csh} varies linearly from 4×10^{-4} s^{-1} to 0 when the corresponding hydrates are totally degraded. Figure 6 shows the profiles of portlandite and calcite for the cement paste with w/c = 0.42, for the three initial average saturations of 0.65, 0.80 and 0.95, and at $t = 25$ days and $t = 225$ days. As expected, the impact of the initial saturation profile appears to be considerable: the degraded zones are indeed much wider (more than twice) in the case where $S_{r|ini} = 0.65$ ($S_{r|ini}$ denotes the initial average saturation in the specimen). Nevertheless, according to the simulations, the maximum intensity of the degradation (in term of maximum volume fraction of precipitated calcite) is quasi-constant whatever $S_{r|ini}$. In Figure 7 are reported both mineralogical XRD profiles (Aït-Mokhtar *et al.*, 2006) and simulated volume fractions of portlandite and calcite for the cases $S_{r|ini} = 0.65$ at $t = 64$ days and $S_{r|ini} = 0.80$ at $t = 180$ days. As the XRD profiles do not directly give quantitative results for solid phase concentrations, they serve here for a qualitative comparison in terms of concentration variations for calcite and portlandite. From this viewpoint, the numerical results appear to agree relatively well the experimental profiles.

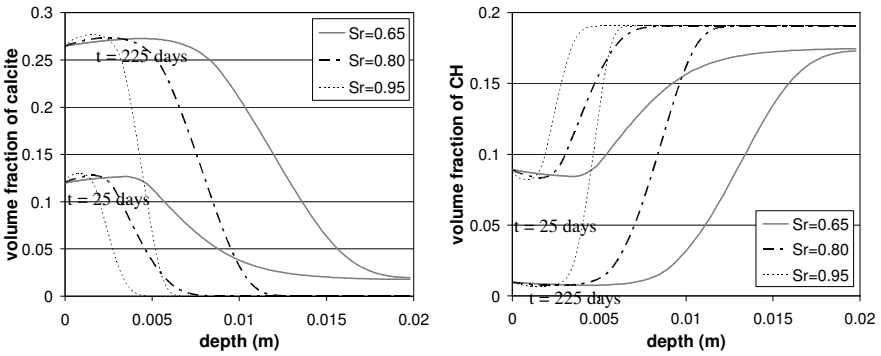

Figure 6. *Numerical profiles of calcite (left) and portlandite (right) for the cement paste with w/c = 0.42, for the initial average saturations of 0.65, 0.80 and 0.95, and for the two times t = 25 days and t = 225 days.*

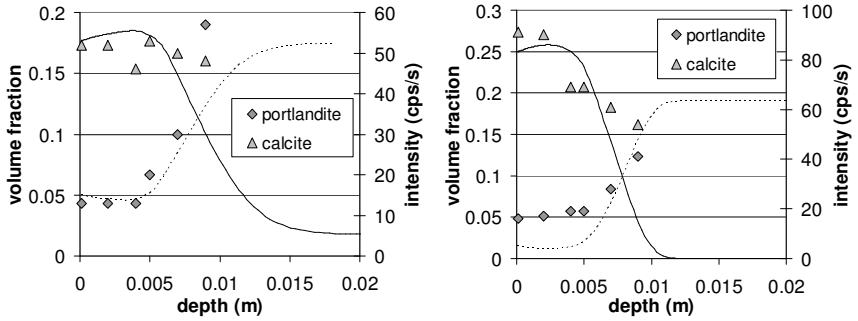

Figure 7. *XRD mineralogical profiles (Aït-Mokhtar et al., 2006) (symbols) and numerical volume fractions (lines) of calcite and portlandite for the cement paste with w/c = 0.42, and the cases* $S_{r|ini}$ *= 0.65 at t = 64 days (left) and* $S_{r|ini}$ *= 0.80 at t = 180 days (right).*

On Figure 8 are displayed the simulated profiles of porosity and saturation degree for the cement paste with w/c = 0.42, for the three initial average saturation of 0.65, 0.80 and 0.95 and at $t = 25$ days and $t = 225$ days. It is recalled here that the initial saturation degree profiles (when tests start) are obtained via the procedure described in section 3.4 and are non homogeneous, whatever the initial average saturation degrees of the materials. The porosity exhibits an important decrease of about 0.08 at $t = 225$ days, showing a progressive filling due to calcite precipitation. This reduction of porosity is consistent with the experimental value reported in (Aït-Mokhtar *et al.*, 2006). Again, it appears clearly that the region affected by the

carbonation is much larger when the initial average saturation degree is low. The examination of the saturation profile evolutions reveals that the water release in the porosity during the degradation mechanisms, combined with the porosity decrease, leads to augment the saturation, in particular in the zones far from the surfaces exposed to drying. It is noteworthy that this increase in water content tends to balance the initially different saturation profiles, in particular in the regions where calcite precipitation occurs. It may then suggest that, since the saturation degree influences significantly the transfer properties (in particular a higher saturation degree implies a lower CO_2 diffusivity), after a sufficient time the global carbonation kinetics for materials having distinct initial saturation conditions become close.

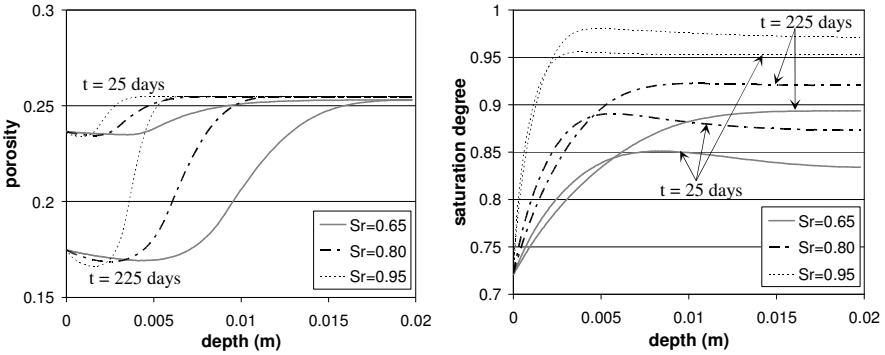

Figure 8. *Numerical profiles of porosity (left) and saturation degree (right) for the cement paste with w/c = 0.42, for the initial average saturations of 0.65, 0.80 and 0.95, and for the two times t = 25 and t = 225 days.*

Figure 9 gathers both experimental and numerical results of carbonation depth for the three cement pastes and the three initial saturation conditions. The simulated depths are estimated on the basis of rather empirical considerations concerning the kinetics of chemical reactions. As already mentioned, it is supposed that the kinetic constant of calcite precipitation from portlandite mainly controls the carbonate concentration in the pore solution, this latter affecting significantly the pH in accelerated test conditions. It is then assumed that the value $k_p = 2\times10^{-3}$ s^{-1}, corresponding to about 25% of the initial portlandite, is approximately equivalent to pH ≈ 9. This value of k_p is adjusted such that the numerical results approach at best the experimental ones for the cement pastes with w/c = 0.42. With this hypothesis, the simulated carbonation depths appear to be in relatively good agreement with experimental data, except for the cases with $S_{r|ini} = 0.95$ where a systematic overestimation is observed. For the cement pastes with w/c = 0.30 and 0.55, the results are also acceptable (more differences appear with the w/c = 0.30

paste), though the kinetic parameters have not been adjusted on the corresponding experimental data.

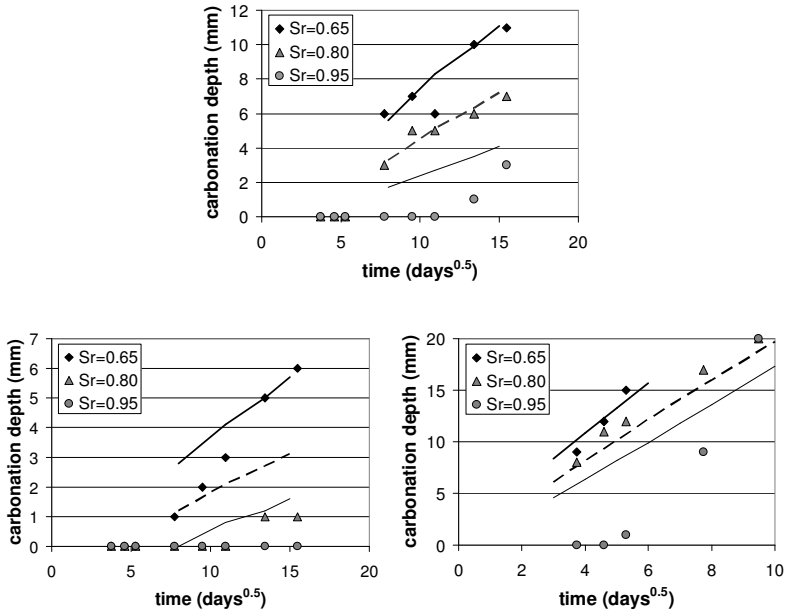

Figure 9. *Numerical (solid lines) and experimental (symbols) carbonation depths for the initial average saturations of 0.65, 0.80 and 0.95, and for the cement pastes with w/c = 0.42 (up), 0.30 (down left) and 0.55 (down right).*

Finally, we present some numerical results concerning the CEM I concrete with w/c = 0.42 and $S_{r|ini}$ = 0.80. Figure 10 depicts the volume fraction profiles of calcite and portlandite at several times from 0 to 225 days. Figure 11 shows, at the same times, the simulated profiles of porosity and saturation degree. The main conclusions mentioned in the case of cement pastes are also valid for concrete. Contrary to the results presented in (Bary *et al.*, 2004), the porosity does not exhibit a total filling at the end of the experiment, although it is considerably reduced (by a factor of about 2) in the zone near the surface exposed to carbonation. This point is of course of major importance because the porosity and the saturation degree are the most significant parameters controlling transfer phenomena. These differences are explained by the much lower calcium migration in pore solution in the case of the present study, meaning that calcite precipitates directly from hydration products (this assumption has allowed to establish the expression of the kinetic constants). Lower calcium concentrations (consecutive to the presence of alkaline ions) combined with reduced concentration gradients (in agreement with the hypothesis of progressive

precipitation mechanisms and in the absence of clear carbonation front) may cause this decrease of calcium flux. These processes are then distinct from the ones occurring in saturated conditions, where carbonation is usually combined with leaching and consequently dissolution and calcium diffusion are of importance. The saturation appears to approach the value 1 in the calcite precipitation zones. If we adopt the method used in the cases of cement pastes for estimating the limit of pH ≈ 9, we obtain a carbonation depth of about 2.5 mm at 225 days, whereas no measurable values have been experimentally reported.

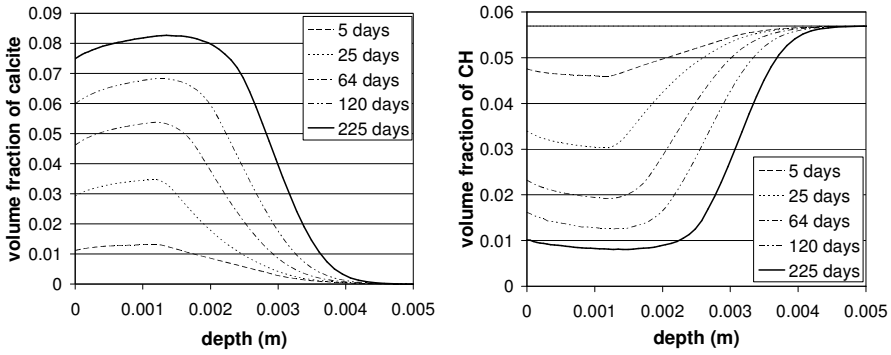

Figure 10. *Numerical profiles of calcite (left) and portlandite (right) at different times for the concrete subjected to accelerated carbonation.*

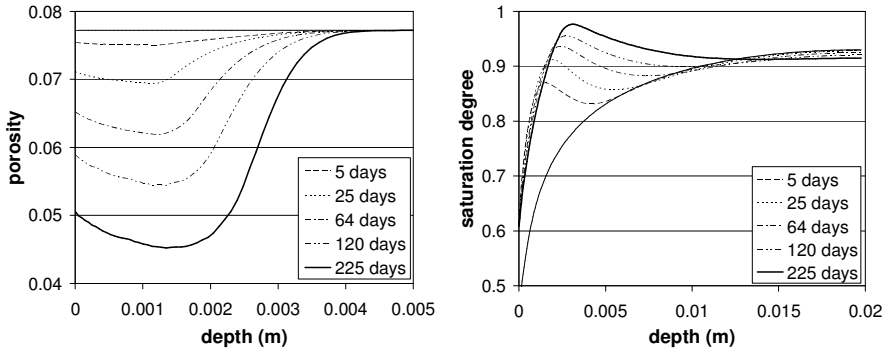

Figure 11. *Numerical profiles of porosity (left) and saturation degree (right) at different times for the concrete subjected to accelerated carbonation.*

5. Conclusion

We have presented in this paper a simplified modelling of cement-based material carbonation in unsaturated conditions, based on the previous study of (Bary *et al.*, 2004). In the new model, more realistic kinetic aspects are introduced in the calcite precipitation, with a distinction between calcite formed from portlandite and from the other hydration products. This distinction rests on the hypothesis that portlandite has a higher initial reactivity, which decreases as the calcite layer surrounding the crystals and constituting a diffusive barrier for ion migration grows. Thus, carbonation reactions do not occur at chemical equilibrium (particularly in the case of accelerated tests), and consequently imply several hydrated phases simultaneously, which is in agreement with experimental observations on accelerated tests. The model parameters are partly calibrated on data available in the literature; most of them are however identified via experiments performed specifically for this study in the workgroup Concrete Engineering Barriers headed by ANDRA. In particular, isotherm adsorption curves have been obtained for all studied materials (CEM I cement pastes with w/c = 0.30, 0.42 and 0.55, and CEM I concrete with w/c = 0.42), and XRD mineralogical profiles have been measured for cement paste with w/c = 0.42 in different configurations. The three resulting governing equations are solved in the Cast3m code by means of a mixed-hybrid finite element method for the space domain and an implicit scheme in time. The model is then applied to the simulation of accelerated carbonation tests carried out on the materials, for three different initial saturation conditions in the case of the pastes. Since complex kinetic aspects on calcite precipitation are introduced in the model, the pH profiles cannot be exactly determined due to our simplified description of chemical equilibriums. Consequently, a method based on a threshold value for the kinetic constant of portlandite is used for estimating the simulated carbonation depths as given by phenolphthalein tests. This method rests on the assumption that once the precipitation of calcite from portlandite reaches a certain level (corresponding precisely to this threshold value of the portlandite kinetic constant), the concentration of carbonate ions becomes in excess with respect to the value at chemical equilibrium (because CO_2 continues to migrate from the outer surface). Indeed, in these conditions the portlandite reaction rate turns out to be much lower than the carbonate flux, leading to increase locally the carbonate concentration and then to significantly decrease the pH. With this hypothesis, the confrontation between computed and experimental results of carbonation depths and mineralogical profiles appears satisfactory. It is worth noticing that in the case of atmospheric carbonation, this method may be adapted because the reactions are likely to occur in quasi-equilibrium conditions. From this point of view, the use of accelerated tests and pH measurements by phenolphthalein for quantitatively estimating the concrete carbonation durability in environmental conditions appears to be questionable. As expected, the initial saturation distributions have an important impact on the global carbonation kinetics; however, it is shown that the water release during the dissolution reactions tends to equilibrate, after a sufficient time, the saturation

degrees in the specimens having different initial conditions. This would suggest that the carbonation kinetics for accelerated tests are likely to become comparable whatever the initial saturation profiles. Though significantly reduced in the carbonated zones and in agreement with experimental observations, the porosity is not completely filled, contrary to the results in (Bary *et al.*, 2004). This dissimilarity is explained by lower calcium concentrations (due to the presence of alkaline ions) and lower calcium flux consecutive to progressive calcite precipitation in larger zones. It is noteworthy that these mechanisms are quite different from the ones occurring in saturated conditions, where carbonation is generally combined with leaching; consequently calcium migration in pore solution is of importance in this case and leads to substantial dissolution and porosity filling.

The next stage will now concern the extension of this modelling to a more complex and complete representation of chemical reactions and involved species in pore solution for the partially saturated materials. This aspect is in progress in CEA via the numerical platform Alliances.

Acknowledgments

Financial support from the French national agency for nuclear waste management (ANDRA) is gratefully acknowledged.

Notations

f	reduction factor for the diffusion of CO_2 [-]
h_r	relative humidity [-]
k	total kinetic coefficient for the reaction of calcite formation [s^{-1}]
k_{csh}	kinetic coefficient of calcite formation from C-S-H [s^{-1}]
k_p	kinetic coefficient of calcite formation from portlandite [s^{-1}]
k_{rl}	relative permeability for liquid [-]
p_c	capillary pressure [Pa]
$p_{\bar{c}}$	partial pressure of carbon dioxide in the gaseous phase [Pa]
p_l	pressure of the liquid phase [Pa]
p_m	pressure of the gaseous phase [Pa]
p_v	partial pressure of the vapour [Pa]
p_{vs}	saturation pressure of the vapour [Pa]
C_a , $C_{\bar{c}}$	calcium and carbonate total concentration in pore solution [mol/m^3]
C_a^* , $C_{\bar{c}}^*$	calcium and carbonate total concentration at chemical equilibrium [mol/m^3]
C_{aS}	concentration of calcium in the initial solid phases [mol/m^3]
D	diffusion coefficient of calcite [m^2/s]
D_a	effective diffusion coefficient of calcium in pore solution [m^2/s]
$D_{\bar{c}}$	diffusion coefficient of CO_2 [m^2/s]
K	intrinsic permeability coefficient [m^2]
K_0	intrinsic permeability coefficient for the material porosity equal to ϕ_0 [m^2]

$M_{\bar{c}}$ molar mass of CO_2 [kg/mol]
M_{H_2O} molar mass of water [kg/mol]
$\dot{N}_{cal}$ molar rate of calcite formation [mol/s/m^3]
R_{p0} initial equivalent radius of portlandite crystals [m]
S_r saturation degree [-]
T temperature [K]
V_{CaCO_3} molar volume of calcite [m^3/mol]
$V_{cal}(t)$ current volume fractions of the precipitated calcite [-]
V_{CH} molar volume of portlandite [m^3/mol]
$V_d(t)$ current volume fractions of the dissolved hydrated products [-]
V_p , V_{p0} current and initial volume fractions of portlandite [-]
$V_{p,\bar{c}}(t)$ volume fraction of portlandite transformed locally in calcite [-]
ϕ porosity [-]
η dynamic viscosity of the water [kg/m/s]
λ parameter interpreted as the initial calcite layer depth when $\kappa_p = 0$ [m]
$\rho_{\bar{c}}$ mass density of CO_2 [kg/m^3]
ρ_l mass density of water [kg/m^3]
ω_{ls} concentration of water chemically bonded in the solid phase [mol/m^3]

6. References

Aït-Mokhtar K., Rougeau P. « Carbonation of high performance concrete for radioactive waste disposal. Part II: Experimental ». To be published in *Revue Européenne de Génie Civil*, 2006.

Atkins P.W., *Physical chemistry*. Sixth Edition, Oxford University Press, Oxford, 1998.

Baroghel-Bouny V., « Caractérisation des pâtes de ciment et des bétons. Méthodes, analyse et interpretations », PhD thesis (in french), LCPC, 1994.

Bary B., Sellier A., « Coupled moisture-carbon dioxide-calcium transfer model for carbonation of concrete », *Cement and Concrete Research*, vol. 34, 2004, p. 1859-1872.

Bary B., Simulation de la carbonatation des matériaux cimentaires de la barrière ouvragée ANDRA en conditions insaturées, Rapport Technique CEA 05-702, 2005.

Bernard O., Uml F.-J., Lemarchand E. « A multiscale micromechanics-hydration model for the eaerly-age elastic properties of cement-based materials », *Cement and Concrete Research*, vol. 33, 2003, p. 1293-1309.

Chaussadent T., Baroghel-Bouny V., Rafaï N., Ammouche A., Hornain H., « Influence du rapport E/C sur l'hydratation, la microstructure et les déformations endogènes de pâtes de ciment durcies », Revue Française de Génie Civil, vol. 5, n°2/3, 2001, P. 217-230.

Dabbene F., « Mixed-hybrid finite elements for transport of pollutants by underground water », *Proc. of the 10th Int. Conf. on Finite Elements in Fluids*, Tucson, USA, 1998.

Fuji K., Kondo W., *Journal of American Ceramics Society*, 57, 1974, p. 492-502.

Groves G.W., Rodway D.I. & Richardson I.G., « The carbonation of hardened cement pastes ». *Advances in Cement Research*, vol. 11, n°3, 1990, p. 117-125.

Ishida T., Maekawa K., Soltani M., « Theoretically identified strong coupling of carbonation rate and thermodynamic moisture states in micropores of concrete », *Journal of Advanced Concrete Technology*, Vol. 2, n°2, 2004, p. 213-222.

Lo Y.; Lee H.M.., « Curing effects on carbonation of concrete using a phenolphthalein indicator and Fourier-transform infrared spectroscopy », *Building & Environment*, Vol. 37 n°5, 2002, p. 507-515.

Mainguy M., Coussy O., Baroghel-Bouny V., « Role of air pressure in drying of weakly permeable materials », *Journal of Engineering Mechanics,* vol. 127 n°6, 2001, p. 582-592.

Millington R. J., « Gas diffusion in porous media », *Science*, vol. 130, 1959, p. 100-102.

Mügler C., « Intégration du modèle de carbonatation atmosphérique des bétons sous Cast3m », Rapport CEA, SFME/MTMS/RT/04-017A, 2004.

Parrott L.J., Killoh D.C., « Carbonation in a 36 year old, in-situ concrete ». *Cement and Concrete Research,* vol. 19, 1989, p. 649-656.

Papadakis V.G., Vayenas C.G., Fardis M.N., « Physical and chemical characteristics affecting the durability of concrete ». *ACI Materials Journal*, vol. 88, n°2, 1991(b), p. 186-196.

Pezzani P. « Propriétés thermodynamiques de l'eau » *Techniques de l'Ingénieur*, K7, n° K585 1988.

Ranznjevic K. *Tables et diagrammes thermodynamiques*, Eyrolles, 1970.

Saetta A. V., Schrefler B. A., Vitaliani R. V., « 2-D model for carbonation and moisture /heat flow in porous materials », *Cement and Concrete Research,* vol. 25 n°8, 1995, p. 1703-1712.

Sercombe J., Vidal R., Adenot F. « Diffusion des gaz dans les ciments. Mécanismes et paramètres principaux », *Proc. of Transfert 2006 Conference*, Lille, 2006.

Thiery M. «Modélisation de la carbonatation atmosphérique des matériaux cimentaires. Prise en compte des effets cinétiques et des modifications microstructurales et hydriques». Thèse de doctorat LCPC (in french), sept. 2005.

van der Lee J., De Windt L., Lagneau V., Goblet P. « Module-oriented modeling of reactive transport with HYTECH » *Computers & Geosciences,* vol. 29, 2003, p. 265-275.

van Genuchten M.T., « A closed-form equation for predicting the hydraulic conductivity of unsaturated soils » *Soil Sci. Soc. Am. Proc.*, vol. 44, 1980, p. 892-898.